

Electrically driven single-photon source at room temperature in diamond

N. Mizuochi^{1,2*}, T. Makino^{3,4}, H. Kato^{3,4}, D. Takeuchi^{3,4}, M. Ogura^{3,4}, H. Okushi^{3,4}, M. Nothafft⁵, P. Neumann⁵, A. Gali^{6,7}, F. Jelezko⁸, J. Wrachtrup⁵ and S. Yamasaki^{3,4}

Single-photon sources that provide non-classical light states on demand have a broad range of applications in quantum communication, quantum computing and metrology¹. Single-photon emission has been demonstrated using single atoms², ions³, molecules⁴, diamond colour centres^{5,6} and semiconductor quantum dots^{7–11}. Significant progress in highly efficient^{8,11} and entangled photons⁹ sources has recently been shown in semiconductor quantum dots; however, the requirement of cryogenic temperatures due to the necessity to confine carriers is a major obstacle. Here, we show the realization of a stable, room-temperature, electrically driven single-photon source based on a single neutral nitrogen-vacancy centre in a novel diamond diode structure. Remarkably, the generation of electroluminescence follows kinetics fundamentally different from that of photoluminescence with intra-bandgap excitation. This suggests electroluminescence is generated by electron-hole recombination at the defect. Our results prove that functional single defects can be integrated into electronic control structures, which is a crucial step towards elaborate quantum information devices.

Single defects in diamonds⁵, particularly single nitrogen-vacancy (NV) centres⁶ (Fig. 1a), have been used as single-photon sources for quantum cryptography¹² and single-photon interference¹³ because of their outstanding photostability at room temperature. The NV centre also exhibits excellent spin characteristics, including long coherence time^{14,15} and fast manipulation rates¹⁶, and allows implementation of few-qubit quantum registers^{17,18}. Coherent coupling between spin and photon¹⁹ and spin-photon entanglement²⁰ have been reported. However, electrical excitation of the NV centre has not been realized. By demonstrating electroluminescence from a single neutral NV centre we have added an additional central element to the quantum toolbox of diamond defects. This provides new opportunities for integrating single-photon sources based on diamond defects into electronic control circuitry and for spintronic applications for quantum communication and processing.

The efficient generation of electroluminescence from diamond single defects requires the synthesis of electron (n-type) and hole (p-type) conducting materials as well as an ultrapure intrinsic (i) layer in a p–i–n diode structure. In the last decade, techniques for diamond semiconductor synthesis including the realization of n-type formation have been developed using microwave plasma-enhanced chemical vapour deposition (CVD)^{21,22}. Diamonds are doped with a large amount of boron and phosphorus to create semi-conducting properties^{21,22}; however, this leads to defects that emit

electroluminescence in the visible spectral range^{21–23}. We therefore introduced an extremely high-quality undoped region to form a p–i–n diamond diode. In previous work we achieved CVD growth of ultrapure intrinsic diamonds, including an isotopically engineered diamond^{14,15,18}, where the concentration of colour centres was reduced to $\ll 0.1$ ppb ($1 \times 10^{13} \text{ cm}^{-3}$), well below the upper limit for single-colour-centre microscopy. In the present work, i- and phosphorus-doped n-type layers were independently grown by CVD on (001) p-type diamond (see Methods). The doping concentrations of phosphorus and boron were $\sim 1 \times 10^{18}$ and $1 \times 10^{19} \text{ cm}^{-3}$, respectively. The electron and hole Hall mobilities were 150 and $10 \text{ cm}^2 \text{ V}^{-1} \text{ s}^{-1}$ at room temperature, respectively. After growth, round mesa structures were fabricated (Fig. 1b) and nitrogen was subsequently implanted, because the i-layer without implantation proved to be too pure to detect native NV centres (concentration of the NV centre is $\ll 1 \times 10^7 \text{ cm}^{-3}$). Measurements were carried out on the NV centres in the i-layer near the edge of the mesa structures (Fig. 1b). The p–i–n diamond, showing an ideal diode characteristic with a rectification ratio of $\sim 1 \times 10^9$ at $\pm 30 \text{ V}$ (Fig. 1c), was investigated for two different surface terminations (hydrogenated and oxidized) of the i-layer²⁴. A homebuilt confocal microscope was used to address single defect centres. All experiments were conducted under ambient conditions.

Photoluminescence raster scans of the intrinsic area were recorded first (Fig. 2a). The photoluminescence spectra indicate the presence of NV centres in a neutral charge state (NV⁰) in the hydrogenated i-layer surface (Fig. 2d) and in a negatively charged state (NV⁻) in the oxidized i-layer surface (Fig. 2c). Antibunching measurements were performed on several NV centres, shown in Fig. 2a and in other regions. Figure 3a shows a typical result of NV⁰ photoluminescence. The second-order autocorrelation function $g^{(2)}(\tau)$ at $\tau = 0$ was less than 0.5, indicating that most NV⁰ photoluminescence in Fig. 2a originated from single centres. The non-zero value of $g^{(2)}(0)$ is considered to be caused mainly by residual photoresist on the surface. In our analysis, the background signal contribution to $g^{(2)}(0)$ was not subtracted. After current injection, electroluminescence was observed from the same region as that of photoluminescence (Fig. 2b) in areas with hydrogenated surfaces. A comparison of Fig. 2a and b reveals that a significant number of NV centres show photoluminescence and electroluminescence. Note that only NV⁰ electroluminescence was observed, even for NV centres that show NV⁻ in photoluminescence. The electroluminescence intensity and temporal stability were sufficiently high to record electroluminescence antibunching (Fig. 3b). A value of $g^{(2)}(0) = 0.45$

¹Graduate School of Engineering Science, Osaka University 1-3, Machikane-yama, Toyonaka-city, Osaka, 560-8531, Japan, ²JST PRESTO, 4-1-8 Honcho Kawaguchi, Saitama, 333-0012, Japan, ³Energy Technology Research Institute-National Institute of Advanced Industrial Science and Technology, Tsukuba, Ibaraki 305-8568, Japan, ⁴JST CREST, 4-1-8 Honcho Kawaguchi, Saitama, 333-0012, Japan, ⁵3rd Physics Institute and Research Center SCoPE, Pfaffenwaldring 57, D-70550 Stuttgart, Germany, ⁶Institute for Solid State Physics and Optics, Wigner Research Centre for Physics, Hungarian Academy of Sciences, Budapest, PO Box 49, H-1525, Hungary, ⁷Department of Atomic Physics, Budapest University of Technology and Economics, Budafoki út 8, H-1111 Budapest, Hungary, ⁸Institut für Quantenoptik, Universität Ulm, Albert Einstein Allee 11, D-89069 Ulm, Germany. *e-mail: mizuochi@mp.es.osaka-u.ac.jp

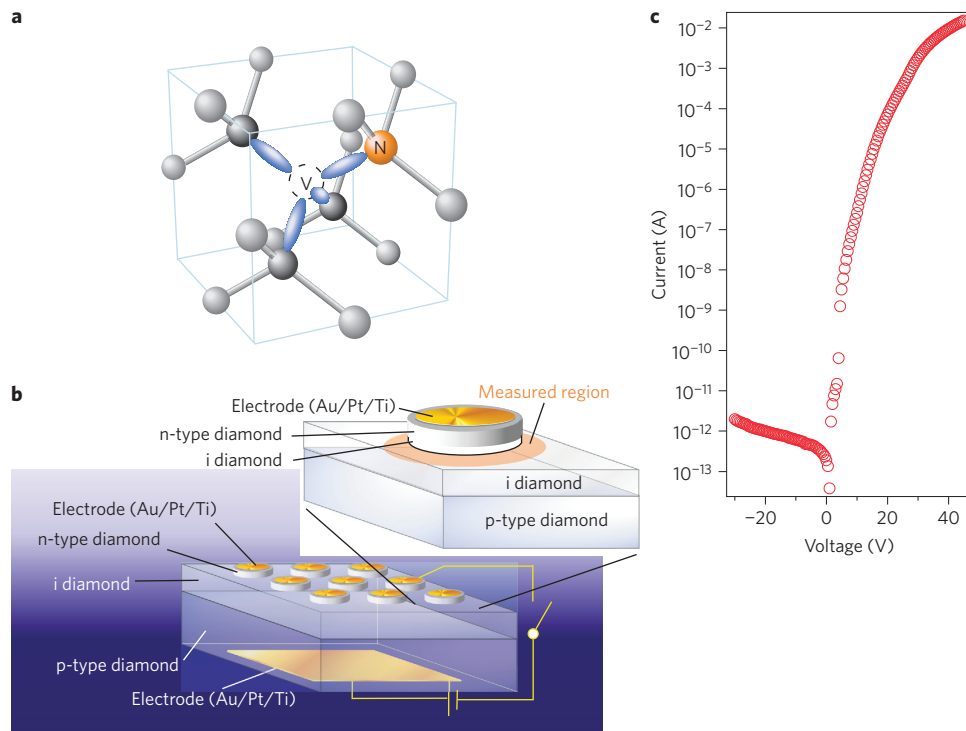


Figure 1 | NV centre in diamond and device. **a**, Atomic structure of an NV centre consisting of a substitutional nitrogen atom and a nearby vacancy in the diamond lattice. **b**, Schematic diagram of the single-photon-emitting diode. The thicknesses of the p-type, intrinsic and n-type layers of the device are 0.5 mm, 10 μm and 0.5 μm, respectively. As a result of dry etching of the n-layer, the thickness of the i-layer was reduced by 200–300 nm. The device was contacted on both interfaces using titanium(30 nm)/platinum(100 nm)/gold(200 nm) electrodes (see Methods). **c**, *I*-*V* properties of the p-i-n junction in a log plot, showing an ideal diode characteristic with a rectification ratio of $\sim 1 \times 10^9$ at ± 30 V. Maximum current densities on the order of 1×10^5 mA cm⁻² were achieved.

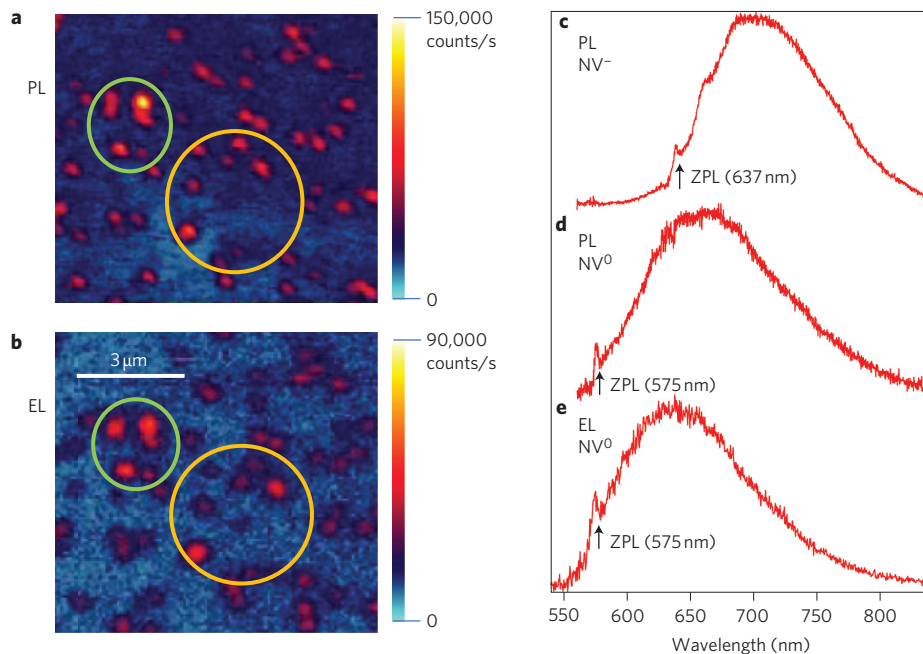


Figure 2 | Microscopy images and spectra. **a,b**, Microscopy images of photoluminescence (PL, **a**) and electroluminescence (EL, **b**). The circles are shown as guide for the eye. The areas in the images are ~ 30 and 40 μm from the edge of the n-layer and the electrodes, respectively. For the photoluminescence measurements, a continuous-wave Nd:YAG laser ($\nu = 532$ nm) was focused on the sample using a high-numerical-aperture (1.4) oil immersion objective. Photoluminescence and electroluminescence were collected by the same objective. Light with wavelengths shorter than 540 nm was rejected by a dichroic mirror to suppress excitation light. **c,d**, Photoluminescence spectra of an NV⁻ centre (**c**) in an oxidized surface diamond and an NV⁰ centre (**d**) in a hydrogenated surface diamond. **e**, Electroluminescence spectrum of a single NV⁰ centre at an applied voltage of 30 V.

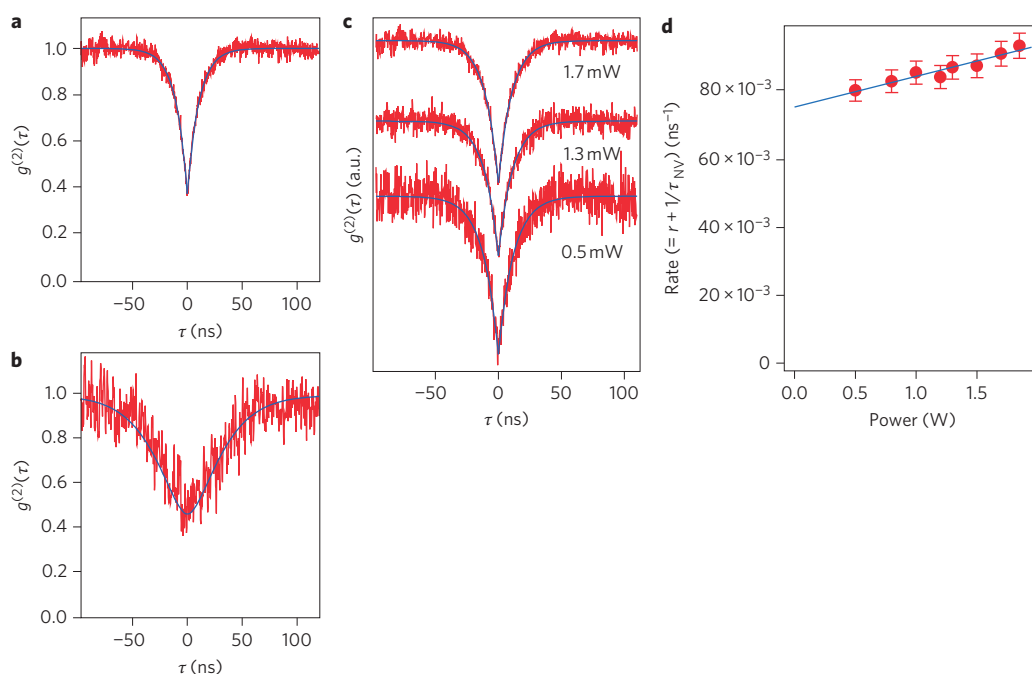


Figure 3 | Antibunching and lifetime of NV^0 . **a,b**, Comparison of photon antibunching statistics induced by photoluminescence (**a**) or electroluminescence (**b**) of a single NV^0 centre. As described in the text, temporal widths of electroluminescence-induced photon antibunching occur on longer timescales than for photoluminescence. **c,d**, Dependence on applied laser power of the rising time of a single NV^0 centre in photoluminescence antibunching. Blue lines in **c** indicate fitting curves for $g^{(2)}(\tau) = 1 - c \exp(-[r + (\tau_{NV})^{-1}]|\tau|)$ in a two-level model. For low laser power ($r \rightarrow 0$), the initial increase of $g^{(2)}(\tau)$ is determined by τ_{NV} . From an extrapolation of the rise time of $g^{(2)}(\tau)$ to $r = 0$ in **d**, τ_{NV} is estimated to be 13.2 ± 0.2 ns.

confirms that the photons originated from a single NV centre. The electroluminescence spectrum was nearly identical to the NV^0 photoluminescence spectrum (Fig. 2e). To the best of our knowledge, this is the first observation of electroluminescence in a single quantum system with photon statistics at room temperature.

In a next step, the dynamics of photoluminescence and electroluminescence excitation and emission were compared. Such a photoluminescence process can be analysed from the temporal width of the dip near zero delay in the $g^{(2)}(\tau)$ data. In a two-level model comprising only ground and excited states, $g^{(2)}(\tau)$ can be approximated as $g^{(2)}(\tau) = 1 - c \exp\{-[r + (\tau_{NV})^{-1}]|\tau|\}$ (ref. 25). (r , pump rate; τ_{NV} , NV^0 lifetime of the excited state; c , constant). The power dependence of $g^{(2)}(\tau)$ from photoluminescence measurements of NV^0 is shown in Fig. 3c,d. For low laser power ($r \rightarrow 0$), the initial increase of $g^{(2)}(\tau)$ is determined by τ_{NV} , which is extrapolated to be 13.2 ± 0.2 ns.

Surprisingly, the temporal dynamics of electroluminescence autocorrelation data differ significantly from those of photoluminescence. Figure 4a shows electroluminescence antibunching curves for various currents (I_{inj}). We investigated several single NV^0 centres and compared electroluminescence and photoluminescence for every centre. All showed the same difference between the electroluminescence and photoluminescence kinetics. In the two-level model, the initial rate of increase of $g^{(2)}(\tau)$ should be determined by τ_{NV} for $I_{inj} \rightarrow 0$ as discussed for photoluminescence. However, the initial rate of increase ($1/\tau'$) of the electroluminescence autocorrelation is apparently slower than $1/\tau_{NV}$ (Figs 3b and 4a). Note that no difference in electroluminescence dynamics was observed between the oxidized and hydrogenated surface conditions. Figure 4c shows the dependence of the initial rate of increase on the injection current, estimated by fitting the single exponential function $g^{(2)}(\tau) = 1 - c \exp\{-|\tau|/\tau'\}$. From the fitted line, τ' at $I_{inj} = 0$ is estimated to be 266^{+218}_{-83} ns. Despite the large error bars, it is evident that this value is non-zero and considerably larger

than the τ_{NV} found in photoluminescence. To interpret the data, we must assume that a third state plays a rate-limiting role in the charge-trapping and emission cycle, which can be qualitatively understood by an additional rate-determining step in consecutive reactions²⁶, as schematically shown in Fig. 4b. Corresponding rate equations are analytically solved (see Supplementary Information). Note that this state is completely different from the metastable singlet state in NV^- centres^{5,6}. In the simulation, k_{21} was constant, with $1/k_{21} = 13.2$ ns. The validity of $1/k_{32} = 266$ ns was also confirmed by the simulation (see Supplementary Information). Simulated $g^{(2)}(\tau)$ functions with constant k_{32} and adjustable parameter k_{13} were fitted to the experimental data (Fig. 4a). From the simulation, k_{13} depends almost linearly on I_{inj} , and was extrapolated to 0 for $I_{inj} \rightarrow 0$ (Fig. 4c).

Figure 4d shows the dependence of electroluminescence intensity on injection current with nonlinear (saturation-type) behaviour. We analysed the saturation of electroluminescence intensity using $I_{EL} = I_{EL,sat}/(1 + P_{sat}/P)^{5,25}$ (I_{EL} , electroluminescence intensity; $I_{EL,sat}$, saturation intensity; P , injected current; P_{sat} , saturation current). From the fit, P_{sat} and $I_{EL,sat}$ were estimated to be 5.3 ± 0.8 mA and 53.8 ± 3.0 kcount/s, respectively. Such a count rate is in agreement with the k_{32} deduced from antibunching measurements when considering the detection efficiency of our experiments to be on the order of a few percentage points.

In indirect-bandgap semiconductors like diamond, indirect recombination via traps, which depends on trap concentration, is dominant. In previous reports on electroluminescence in diamond devices, a strong free-exciton emission at 235 nm and a weak broad emission of band A around ~ 350 – 600 nm due to traps were observed²². In our device, no strong signal was observed in band A at wavelengths longer than 540 nm (Fig. 2e), indicating that the NV^0 emission caused by absorption of photons is unlikely. Most importantly, the significantly different behaviour of photon antibunching for photoluminescence and electroluminescence proves

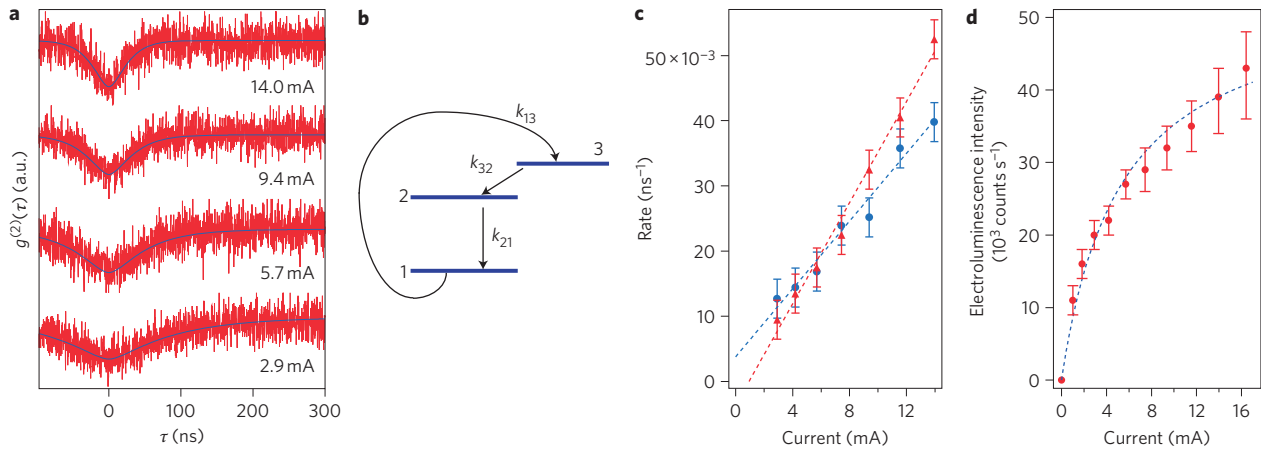


Figure 4 | Kinetics of electroluminescence. **a**, Measured dependence on injection current of electroluminescence antibunching of NV^0 . Blue lines are results of simulations of a three-level model with constants $1/k_{21} = \tau_{\text{NV}} = 13.2$ ns and $1/k_{32} = 266$ ns and fitting parameter k_{13} . Details of the simulation are described in the Methods. **b**, Schematic model of the dynamics, in which k_{13} represents electrical pumping to level 3, followed by a rate-determining step (k_{32}) to level 2. Levels 1 and 2 are the ground and excited states of NV^0 , respectively. **c**, Measured dependence of the initial increase (blue filled circles = $1/\tau$) of electroluminescence autocorrelation data on the injection current, estimated by fitting of a single exponential function $g^{(2)}(\tau) = 1 - c \exp\{-|\tau|/\tau\}$. Blue dotted line is a fit to the data. Excitation rate k_{13} is derived for each current from a simulation with conditions where $1/k_{21} = \tau_{\text{NV}} = 13.2$ ns and $1/k_{32} = 266$ ns, shown as red filled triangles. Red dotted line is a fit to these conditions. **d**, Measured dependence of electroluminescence intensities on injection current. Experimental data are shown by red circles. Blue dotted curve is a fitting curve showing saturation behaviour, as described in the text.

that electroluminescence cannot be excited by photon absorption by the NV centre. We therefore conclude that electroluminescence of the NV centre is instead excited by carrier recombination at the defect site, caused either by individual charges or free excitons, similar to the electroluminescence process of nitrogen in GaP^{27} .

To quantitatively see how efficiently the NV centre can act as a recombination centre for carriers, the effective charge carrier trapping rate (pumping rate, k_{13}) was estimated by Shockley–Read–Hall (SRH) statistics and Langevin recombination (see Methods). The values derived by SRH and Langevin models differ, being $k_{13}^{-1} = 20$ ns and 4.3 ns, respectively, for an injection current of 4 mA (see Supplementary Information). As Fig. 4c shows, $(k_{13})^{-1}$ at 4 mA was measured to be ~ 80 ns, which is longer than the calculated values. We attribute this to our device design (see Methods). Furthermore, our kinetic model is consistent with the linear dependence of k_{13} on injected current (Fig. 4c), in accordance with the recombination models.

A tentative explanation for the different kinetics of electroluminescence and photoluminescence can be drawn from *ab initio* calculations, attributing the additional state 3 and the rate k_{32} to an $S = 3/2$ excited state of a loosely bound hole in the valence band edge and a strongly bound electron on NV^0 (see Supplementary Information). This state has energy (~ 2.3 eV) very close to the zero-phonon line of NV^0 , so it can decay from this state to the 2A_1 excited state via spin–orbit coupling, which decays to the 2E ground state²⁸. Free excitons in intrinsic high-purity diamond have a long lifetime (see Methods) and can therefore diffuse to a far region²². This explanation is based on exciton recombination, but we do not exclude other possibilities in view of the lack of direct experimental evidence.

The mechanism we invoke for electroluminescence is considered to be similar to that of cathodoluminescence. Because cathodoluminescence of NV^- was observed²⁹, the electroluminescence of NV^- is considered possible. Around the NV, many holes are present because of the high concentration of boron ($\sim 1 \times 10^{19}$ cm^{-3}) compared with phosphorus ($\sim 1 \times 10^{18}$ cm^{-3}). Thus, it may be possible to observe the electroluminescence of NV^- by increasing the concentration of phosphorus. Theory²⁸ and experiments³⁰ have shown that NV^0 has unpaired electron spins with long lifetimes, which are required for spintronics applications.

Currents up to 14 mA and photon emission rates of more than 4×10^4 photons/s were observed (Fig. 4d). Charge injection with milliamp currents increases the temperature, which may lead to lower-efficiency electroluminescence. We expect to observe higher emission rates by refining our structure design. In this study, NV centres are not located below the electrode, which decreases the current density at the defect site. By integrating electrodes into the nanowire structures²⁵, the emission intensity can be expected to increase significantly as a result of confinement of the charge carriers to a narrower conduction channel and an increase in the light collection efficiency. The emission intensity at ambient conditions is therefore expected to approach the levels ($\sim 1 \times 10^7$ counts/s)¹¹ known from quantum dots. In addition, such structures might pave the way to the development of diamond-based room-temperature spintronics devices.

Note added in proof: During the review process we became aware of independent research about electroluminescence from a single NV^0 in a light-emitting diode made by ion implantation, which was submitted after our submission and has now been published³¹.

Methods

Synthesis of p–i–n diamond. Phosphorus-doped n-type and i-layers were independently grown by CVD on high-pressure high-temperature synthetic IIb (001) p-type single-crystalline diamond. For CVD growth, the input microwave powers and CH_4/H_2 ratio for the i- and n-type films were 4,200 W, 750 W and 4.0%, 0.4%, respectively. Gas pressures for the i- and n-type films were 170 and 25 torr, respectively. Substrate temperatures in the i- and n-type films were kept constant at 850 °C and 900 °C. For the i-layer, O_2 was added into the feeding gas at a ratio (O_2/CH_4) of 2.5% to reduce the contamination from boron and other impurity atoms. For the n-type layer, PH_3 diluted with H_2 was used for phosphorus doping at a ratio (PH_3/CH_4) of 5%. The thickness of the IIb substrate, i-layer and n-type layers were 0.5 mm, 10 μm and 0.5 μm , respectively. The thickness of the i-layer etched away as a result of the dry etch of the n-layer was ~ 200 – 300 nm.

After growth, round mesa structures with a diameter of 220 μm were fabricated by conventional photolithography and inductively coupled plasma etching processes. Nitrogen was ion-implanted with a density of 1×10^9 atoms/ cm^2 and kinetic energy of 180 keV, leading to implantation to a depth of 300 nm. Annealing at 800 °C for 1 h produced NV centres. Nitrogen was implanted into all areas of the sample, including into the n-type film. However, no change in electrical properties such as the *I*–*V* characteristics was detected after nitrogen implantation, because the concentration of implanted nitrogen (1×10^{13} cm^{-3}) was negligible compared to that of phosphorus. The p–i–n junction layers were kept in a mixture of H_2SO_4 and HNO_3 at 200 °C for 60 min to remove surface contamination and to terminate the surface with oxygen. Titanium(30 nm)/platinum(100 nm)/gold(200 nm) electrodes

with diameters of 200 μm and square areas of 1.5 mm \times 1.5 mm were formed on the n-type layer and the 11b substrate, respectively. Electrodes on the n-type layer were connected by gold wire, and the electrode on the p-type film was attached to a copper plate. Hydrogenation of the surface was performed using H_2 radical irradiation for 10 min at 4 kPa by means of a hot filament system, which also removed residual photoresist material from creating the electrodes on the mesa structures. The flow of highly pure H_2 gas (99.9999999%) was 400 s.c.c.m. The temperature of the sample was kept below 550 $^\circ\text{C}$ during the hydrogenation procedure. Oxidation was performed by inductively coupled plasma O_2 gas, which was also used to remove residual photoresist material in a careful manner so as not to damage the electrode. After surface cleaning processes, the signal-to-background ratio was sufficiently high to indicate whether $g^{(2)}(0)$ was smaller than 0.5. The sample was annealed at 420 $^\circ\text{C}$ for 30 min in an argon atmosphere. All electrical properties were measured in vacuum at room temperature.

Analysis of recombination rate. Recombination in high-mobility material is generally analysed using SRH statistics²⁷. However, the Langevin recombination model considers the Coulomb interaction process to capture carriers and is usually applied to low-mobility materials. As we expect charge injection with milliamp currents to significantly enhance the temperature of our device, we are probably in a situation of lower mobility of high currents (see Supplementary Information). We therefore estimate the recombination rate by the two models and exemplify the calculation for the SRH model. In particular, the NV centre is located in the i-layer and the distance of the NV centre from the edge of the n-layer is $\sim 30 \mu\text{m}$ at a depth of $\sim 300 \text{ nm}$. Therefore, a smaller carrier concentration could be responsible for the slower pumping rate in the experiment (see Supplementary Information). Nevertheless, both models give a realistic estimate of the effective excitation rate and show that charge carrier recombination is a possible mechanism for electroluminescence, in contrast to impact ionization (see Supplementary Information).

Received 8 August 2011; accepted 5 March 2012;
published online 15 April 2012

References

- Santori, C., Fattal, D. & Yamamoto, Y. *Single-Photon Devices and Applications* (Wiley, 2010).
- Kuhn, A., Hennrich, M. & Rempe, G. Deterministic single-photon source for distributed quantum networking. *Phys. Rev. Lett.* **89**, 067901 (2002).
- Keller, M., Lange, B., Hayasaka, K., Lange, W. & Walther, H. Continuous generation of single photons with controlled waveform in an ion-trap cavity system. *Nature* **431**, 1075–1078 (2004).
- Lounis, B. & Moerner, W. E. Single photons on demand from a single molecule at room temperature. *Nature* **407**, 491–493 (2000).
- Kurtsiefer, C., Mayer, S., Zarda, P. & Weinfurter, H. Stable solid-state source of single photons. *Phys. Rev. Lett.* **85**, 290–293 (2000).
- Aharonovich, I. et al. Diamond-based single-photon emitters. *Rep. Prog. Phys.* **74**, 076501 (2011).
- Michler, P. et al. A quantum dot single-photon turnstile device. *Science* **290**, 2282–2285 (2000).
- Yuan, Z. et al. Electrically driven single-photon source. *Science* **295**, 102–105 (2002).
- Salter, C. L. et al. An entangled-light-emitting diode. *Nature* **465**, 594–597 (2010).
- Kako, S. et al. A gallium nitride single-photon source operating at 200 K. *Nature Mater.* **5**, 887–892 (2006).
- Strauf, S. et al. High-frequency single-photon source with polarization control. *Nature Photon.* **1**, 704–708 (2007).
- Beveratos, A. et al. Single photon quantum cryptography. *Phys. Rev. Lett.* **89**, 187901 (2002).
- Jacques, V. et al. Experimental realization of Wheeler's delayed-choice gedanken experiment. *Science* **315**, 966–968 (2007).
- Mizuochi, N. et al. Coherence of single spins coupled to a nuclear bath of varying density. *Phys. Rev. B* **80**, 041201(R) (2009).
- Balasubramanian, G. et al. Ultralong spin coherence time in isotopically engineered diamond. *Nature Mater.* **8**, 383–387 (2009).
- Fuchs, G. D. et al. Gigahertz dynamics of a strongly driven single quantum spin. *Science* **326**, 1520–1522 (2009).
- Dutt, M. V. G. et al. Quantum register based on individual electronic and nuclear spin qubits in diamond. *Science* **316**, 1312–1316 (2007).
- Neumann, P. et al. Multipartite entanglement among single spins in diamond. *Science* **320**, 1326–1329 (2008).
- Buckley, B. B., Fuchs, G. D., Bassett, L. C. & Awschalom, D. D. Spin-light coherence for single-spin measurement and control in diamond. *Science* **330**, 1212–1215 (2010).
- Togan, E. et al. Quantum entanglement between an optical photon and a solid-state spin qubit. *Nature* **466**, 730–735 (2010).
- Koizumi, S., Watanabe, K., Hasegawa, M. & Kanda, H. Ultraviolet emission from a diamond pn junction. *Science* **292**, 1899–1901 (2001).
- Makino, T. et al. Enhancement in emission efficiency of diamond deep-ultraviolet light emitting diode. *Appl. Phys. Lett.* **99**, 061110 (2011).
- Zaitsev, A. M., Bergman, A. A., Gorokhovskiy, A. A. & Huang, M. Diamond light emitting diode activated with Xe optical centers. *Phys. Status Solidi (a)* **203**, 638–642 (2006).
- Hauf, V. et al. Chemical control of the charge state of nitrogen-vacancy centers in diamond. *Phys. Rev. B* **83**, 081304(R) (2011).
- Babinec, T. M. et al. A diamond nanowire single-photon source. *Nature Nanotech.* **5**, 195–199 (2010).
- Watkins, P. W. *Physical Chemistry* 4th edn, ch. 26 (Oxford Univ. Press, 1989).
- Sze, S. M. et al. *Physics of Semiconductor Devices* (Wiley-Interscience, 2006).
- Gali, A. Theory of the neutral nitrogen-vacancy center in diamond and its application to the realization of a qubit. *Phys. Rev. B* **79**, 235210 (2009).
- Watanabe, H., Kitamura, T., Nakashima, S. & Shikata, S. Cathodoluminescence characterization of a nitrogen-doped homoepitaxial diamond thin film. *J. Appl. Phys.* **105**, 093529 (2009).
- Felton, S. et al. Electron paramagnetic resonance studies of the neutral nitrogen vacancy in diamond. *Phys. Rev. B* **77**, 081201 (2008).
- Lohrmann, A. et al. Diamond based light-emitting diode for visible single-photon emission at room temperature. *Appl. Phys. Lett.* **99**, 251106 (2011).

Acknowledgements

The authors acknowledge financial support by the Japan Science and Technology Agency (JST) Precursory Research for Embryonic Science and Technology (PRESTO) programme, as well as KAKENHI (grant nos 22102502 and 23681017), the Strategic Information and Communication R&D Promotion Program (SCOPE), the National Institute of Information and Communications Technology (NICT) programme, the JST Core Research for Evolutional Science and Technology (CREST) programme, the European Union (EU) via the grants Solid State Quantum Technology and Metrology Using Spins (SQUTEC), DIAMANT and Solid State Systems for Quantum Information Processing (SOLID), the Deutsche Forschungsgemeinschaft (DFG) via research groups 730, 1482 and 1495, the Max Planck Society, and the Hungarian Scientific Research Fund (OTKA; grant no. K-67886).

Author contributions

T.M., H.K., D.T. and M.O. synthesized and fabricated the diamond device. N.M. built a home-made confocal microscope system with assistance from P.N., F.J. and J.W., and carried out the measurements. N.M., M.N., H.O., S.Y., P.N., F.J. and J.W. contributed to the data analysis. A.G. carried out group theory analysis and the *ab initio* calculations. N.M. and J.W. wrote the manuscript with feedback from all authors. All authors discussed the results and commented on the manuscript.

Additional information

The authors declare no competing financial interests. Supplementary information accompanies this paper at www.nature.com/naturephotonics. Reprints and permission information is available online at <http://www.nature.com/reprints>. Correspondence and requests for materials should be addressed to N.M.